scientific reports

OPEN

Returning long-range PM$_{2.5}$ transport into the leeward of East Asia in 2021 after Chinese economic recovery from the COVID-19 pandemic

Syuichi Itahashi[1]✉, Yuki Yamamura[2], Zhe Wang[3] & Itsushi Uno[4]

Changes in the aerosol composition of sulfate (SO$_4^{2-}$) and nitrate (NO$_3^-$) from 2012 to 2019 have been captured as a paradigm shift in the region downwind of China. Specifically, SO$_4^{2-}$ dramatically decreased and NO$_3^-$ dramatically increased over downwind locations such as western Japan due to the faster reduction of SO$_2$ emissions than NO$_x$ emissions and the almost constant trend of NH$_3$ emissions from China. Emissions from China sharply decreased during COVID-19 lockdowns in February–March 2020, after which China's economic situation seemed to recover going into 2021. Given this substantial change in Chinese emissions, it is necessary to clarify the impact of long-range PM$_{2.5}$ transport into the leeward of East Asia. In this study, ground-based aerosol compositions observed at three sites in western Japan were analysed. The concentrations of PM$_{2.5}$, SO$_4^{2-}$ and NO$_3^-$ decreased in 2020 (during COVID-19) compared with 2018–2019 (before COVID-19). In 2021 (after COVID-19), PM$_{2.5}$ and NO$_3^-$ increased and SO$_4^{2-}$ was unchanged. This suggests the returning long-range PM$_{2.5}$ transport in 2021. From numerical simulations, the status of Chinese emissions during COVID-19 did not explain this returning impact in 2021. This study shows that the status of Chinese emissions in 2021 recovered to that before COVID-19.

Before the outbreak of COVID-19, strong emission regulations in China had led to a rapid decrease in PM$_{2.5}$ concentrations from 2013[1–3], and this improvement in Chinese PM$_{2.5}$ pollution was associated with improved air quality in terms of PM$_{2.5}$ over the region downwind of China in 2010–2019[4]. Moreover, nitrate aerosol (NO$_3^-$) became an important component of PM$_{2.5}$ by replacing sulfate aerosol (SO$_4^{2-}$), which had previously dominated aerosol pollution over East Asia[5,6]. This feature is recognised as a paradigm shift in PM$_{2.5}$ composition. Such variations with increasing importance of NO$_3^-$ were also found from long-term analyses of the precipitation chemistry over East Asia[7,8]. These changes were due to the different reduction rates of NO$_x$ and SO$_2$ emissions with the faster reduction in SO$_2$ emission and the steadily high rate of NH$_3$ emission in China. This trend was expected to continue.

However, unexpected changes in air quality occurred because of the COVID-19 outbreak in December 2019 in the city of Wuhan in Hubei, China[9]. In response to the pandemic, lockdowns were imposed on many cities in China during February and March 2020, and these measures limited human activities such as travel and economic activity[10,11]. Accordingly, strong reductions in anthropogenic emissions were estimated[12] and observed[13–17], and subsequent improvements in air pollution were reported over China[18,19]. Because the long-range transport (i.e., trans-boundary transport) of air pollutants in East Asia is an important environmental issue[20,21], the reduction in anthropogenic emissions in China during COVID-19 will further impact the changes in air pollution over not only China but also downwind regions such as the Korean Peninsula and Japan. This leads to another question: How is the situation after COVID-19? Based on China's estimated GDP, its economy has recovered
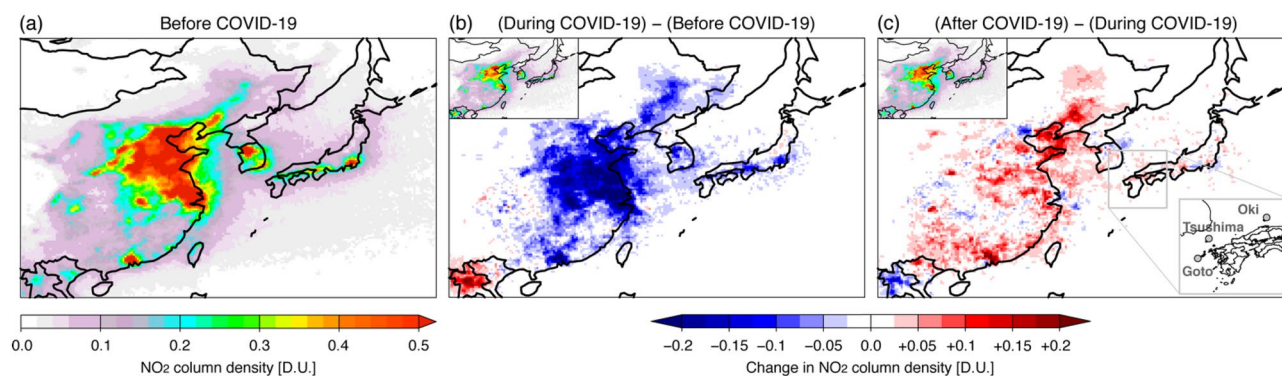
Figure 1. Satellite-measured tropospheric NO_2 column density over East Asia: (**a**) before COVID-19; (**b**) difference between during COVID-19 and before COVID-19; (**c**) difference between after COVID-19 and during COVID-19. The analysed period is the average of February and March. The inset in the upper left of (**b**) and (**c**) shows the absolute values during and after COVID-19, respectively. The inset in the lower right of (**c**) shows the three observation sites analysed in this study. The maps were generated with gtool3 (http://www.gfd-dennou.org/library/gtool/index.htm.en).

since the 2020 lockdowns and is projected to keep growing[22]. Unlike the OECD countries, China achieved positive GDP growth in 2020, and this economic recovery likely led to a rebound in anthropogenic emissions. Against this background, it is worth investigating and clarifying, from the perspective of the downwind region, the changes in long-range transport that resulted from the substantial emission changes that happened before, during and after COVID-19 in China. In the present study, we analysed the changes in aerosol components over the leeward of East Asia based on a combination of ground-based and satellite observations and sensitivity experiments in numerical modeling simulations.

Results

We analysed aerosol compositions for February and March in each year from 2018 to 2021. For simplicity in the following discussion, 2018, for example, stands for the average in February and March in 2018. These two months (February and March) corresponded to COVID-19 lockdown periods in China in 2020[16] and so are considered as the most suitable period for evaluating the change in $PM_{2.5}$ pollution before, during and after COVID-19. Herein, we refer to the two-year average for 2018 and 2019 as before COVID-19, 2020 as during COVID-19 and 2021 as after COVID-19. Figure 1 shows the NO_2 column over East Asia as measured by the Ozone Monitoring Instrument (OMI) (see "Methods") before, during, and after COVID-19. A high NO_2 column was found over north-eastern China before COVID-19 (Fig. 1a). Compared with its before-COVID-19 status, the NO_2 column decreased dramatically during COVID-19 over the whole of eastern China (Fig. 1b). Then, although some parts showed decreases, almost all parts of China showed an increased NO_2 column after COVID-19 compared to during COVID-19 (Fig. 1c). These satellite results suggest substantial deceases in emissions over China in 2020 and then increased emissions along with the economic recovery in 2021.

Figure 2 shows the observational results of mean, 75 percentile (3Q), median, and 25 percentile (1Q) for changes in $PM_{2.5}$ and its composition at three remote sites in Goto, Tsushima, and Oki located in western Japan (see the lower-right corner of Fig. 1c) from 2018 to 2021. At each of these three sites, an aerosol chemical speciation analyszer (ACSA) measured the $PM_{2.5}$, SO_4^{2-} and NO_3^- concentrations (see "Methods"). Because the NO_3^- concentration had a high peak in a short time and was otherwise generally close to zero, the mean value is sometimes higher than the 3Q value. In addition to the concentration analyses in Fig. 2, changes in the concentration of $PM_{2.5}$ and its composition (denoted as C) during and after COVID-19 are further illustrated in Fig. 3 based on the following equations:

$$\text{Change in } C_{\text{during COVID-19}} \ [\%] = \frac{C_{\text{during COVID-19}} - C_{\text{before COVID-19}}}{C_{\text{before COVID-19}}} \times 100, \tag{1}$$

$$\text{Change in } C_{\text{after COVID-19}} \ [\%] = \frac{C_{\text{after COVID-19}} - C_{\text{during COVID-19}}}{C_{\text{during COVID-19}}} \times 100. \tag{2}$$

The observational results (Figs. 2 and 3) show that the $PM_{2.5}$, SO_4^{2-} and NO_3^- concentrations decreased substantially during compared with before COVID-19. The SO_4^{2-} concentration decreased gradually from 2018 to 2020, whereas the NO_3^- concentration increased from 2018 to 2019 and then decreased from 2019 to 2020. The increase in NO_3^- concentration in 2019 found at Goto and Oki was consistent with our previous study that reported the change in aerosol composition as a paradigm shift[4]. In 2021, increases in $PM_{2.5}$ and NO_3^- and almost the same level of SO_4^{2-} have been measured. Considering the expected economic recovery suggested from the NO_2 column (Fig. 1c), the returning impact of long-range transport can be assumed. However, because $PM_{2.5}$ concentration and composition can also be affected by the meteorological field and emission sources other than
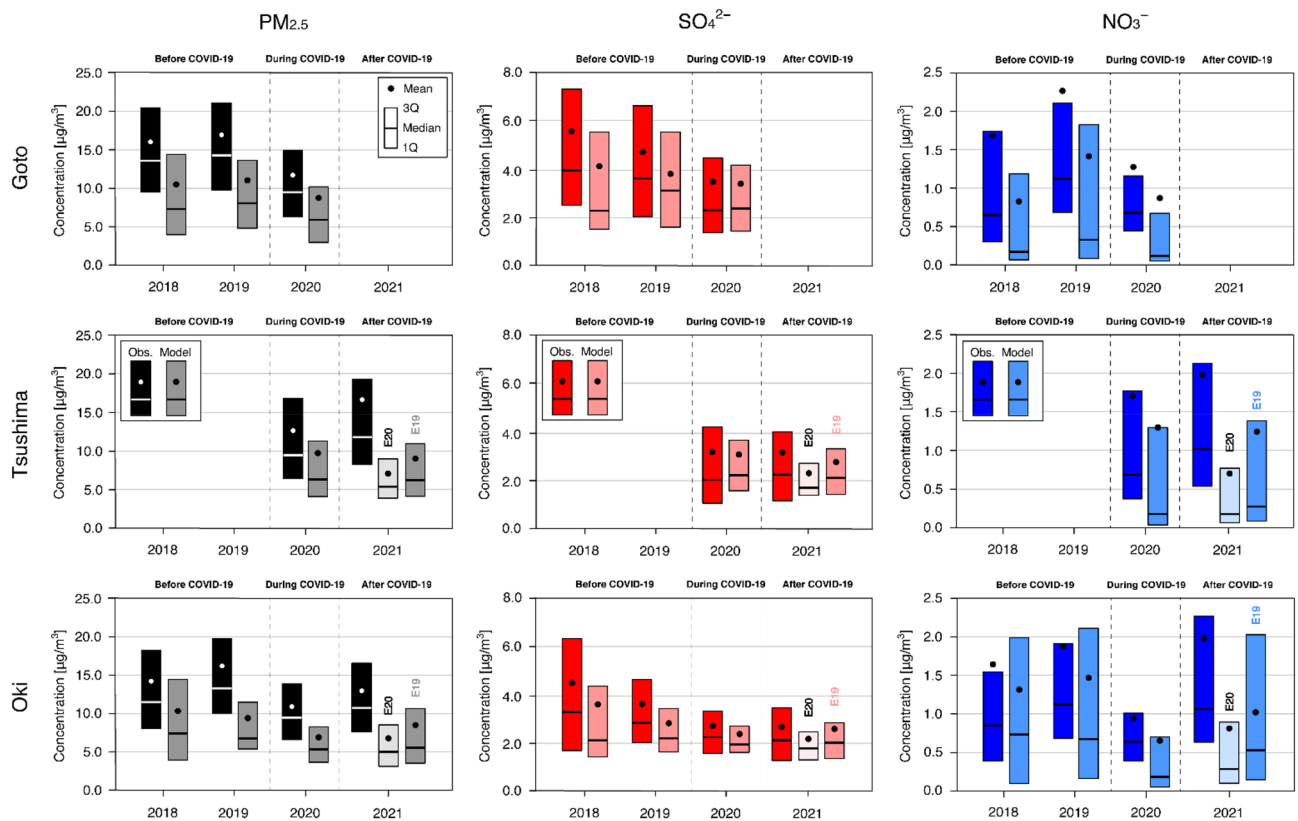
Figure 2. Two-month (February and March) average of (left) PM$_{2.5}$, (centre) SO$_4^{2-}$ and (right) NO$_3^-$ concentrations from 2018 to 2021 at (top) Goto, (middle) Tsushima and (bottom) Oki. For each year, the observation is shown on the left and the model is shown on the right. For 2021, the model experiments of M21E20 and M21E19 are shown by the lighter colour and darker colour and denoted as E20 and E19, respectively.

anthropogenic sources, further discussion is required, and we conducted modeling simulations to clarify this point.

Discussion

To identify a potential reason for the variation in air pollutants found in 2021, we conducted numerical simulations for 2018–2021. The experiments are described in Table 1 (see "Methods" for details about the modeling configurations). In the names of these experiments, 'M' and 'E' denote meteorology and Chinese anthropogenic emissions, respectively (e.g., M18E18 indicates the meteorological field for 2018 and the emission inventory for 2018). From 2018 to 2020, the meteorological field and available emissions corresponding to the simulation periods were used. Through comparison with ACSA observations for 2018–2020 (Figs. 2 and 3), we confirmed that the model generally captured the observed variations of PM$_{2.5}$, SO$_4^{2-}$ and NO$_3^-$ concentrations. Statistical analyses were conducted to evaluate the modeling performance based on the correlation coefficient (R), the normalised mean bias (NMB) and the normalised mean error (NME), and the modeling performance was judged based on metrics from a review of modeling applications (see "Methods" for definitions). The results of the statistical analyses are given in Table 2. For PM$_{2.5}$, the model showed moderate correlation with observations but tended to underestimate the observed concentration; in some cases, the criteria for acceptable model performance were judged as not having been met. This underestimation stemmed mainly from the underestimation of organic aerosol in comparison with a model intercomparison study[23]. For SO$_4^{2-}$ and NO$_3^-$, the model also tended to underestimate the observed concentrations, but in most cases it was judged to have performed well within the criteria. The model's underestimation for SO$_4^{2-}$ was due to the insufficient oxidation process in the current modeling[24]. Considering our previous findings from a model intercomparison study in Japan[25], one of the possible reasons for the model's underestimation for NO$_3^-$ was the uncertainty of NH$_3$ emissions. In addition to emissions, partitioning between fine- and coarse-mode NO$_3^-$, and also the thermodynamic equilibrium between fine-mode NO$_3^-$ and gas-phase nitric acid (HNO$_3$), would be an important aspect to refine the modeling performance on fine-mode NO$_3^{-}$[26].

For 2021, two experiments were conducted because of the lack of emission information for that year (Table 1). In these experiments, anthropogenic emissions from China have been perturbed. One was M21E20, using the meteorological field for 2021 but the Chinese emissions for 2020 (as during COVID-19) with the natural emissions for 2021; the other was M21E19, also using the meteorological field for 2021 but now the Chinese emissions for 2019 (as before COVID-19) with the natural emissions for 2021. Based on these two experiments, the impact
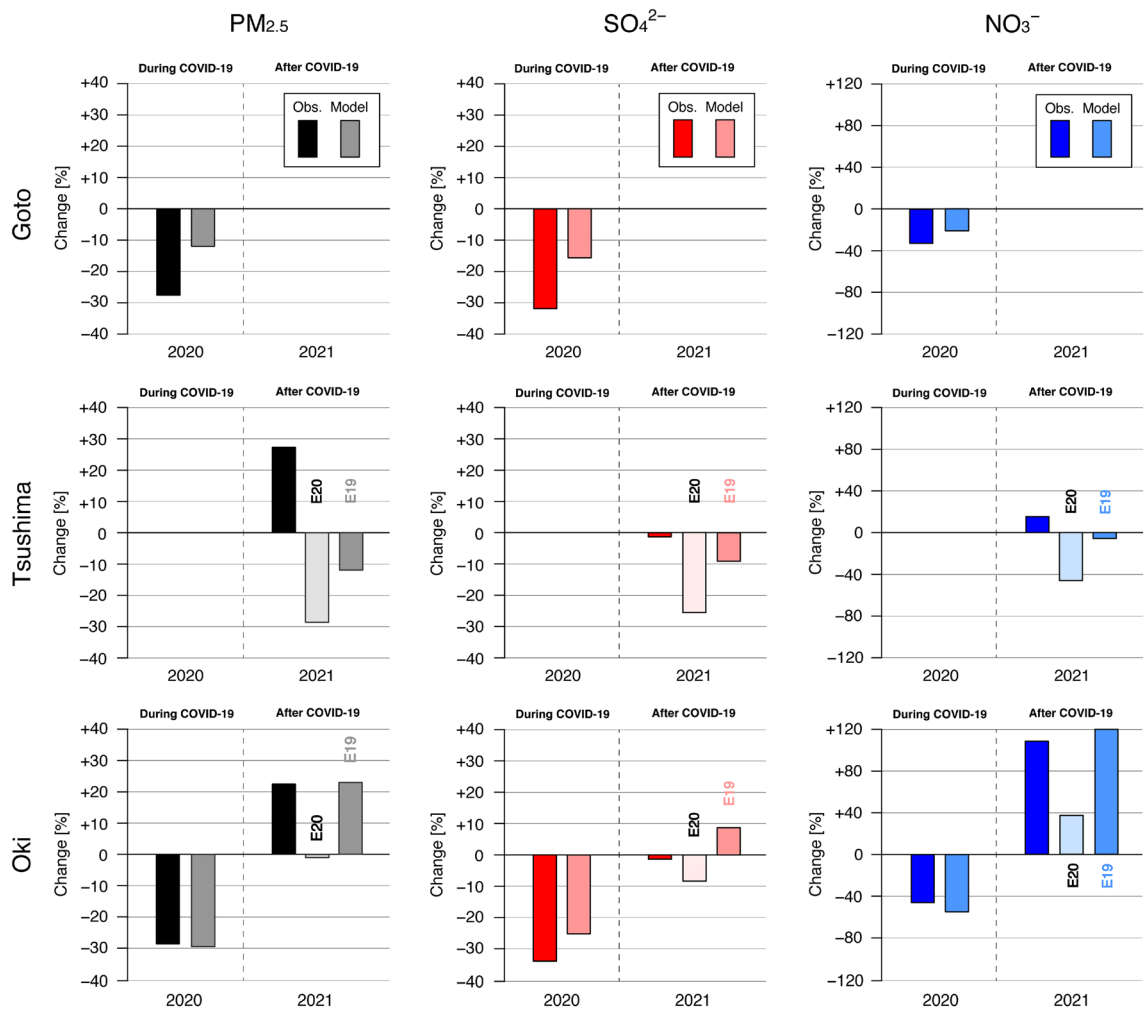
Figure 3. Changes in two-month (February and March) averaged (left) PM$_{2.5}$, (centre) SO$_4^{2-}$ and (right) NO$_3^-$ concentrations during and after COVID-19 at (top) Goto, (middle) Tsushima and (bottom) Oki. These were calculated from the mean values in Fig. 2. For each year, the observation is shown on the left and the model is shown on the right. For 2021, the model experiments of M21E20 and M21E19 are shown by the lighter colour and darker colour and denoted as E20 and E19, respectively.

Modeling experiment	Meteorology	Anthropogenic emissions from China	Ship emissions	Natural emissions (biomass burning, biogenic and volcanoes)	Purpose
M18E18	2018	2018	2010	2018	Simulation using meteorology and emissions for 2018
M19E19	2019	2019	2010	2019	Simulation using meteorology and emissions for 2019
M20E20	2020	2020	2020	2020	Simulation using meteorology and emissions for 2020
M21E20	2021	2020	2020	2021	Simulation using meteorology and fixed Chinese emissions in 2020 for 2021 assuming the emission levels during COVID-19
M21E19	2021	2019	2020	2021	Simulation using meteorology and fixed Chinese emissions in 2019 for 2021 assuming the emission levels before COVID-19

Table 1. Description of present modeling experiments ('M' and 'E' denote meteorology and Chinese anthropogenic emissions, respectively).

Location	Pollutant	Metrics	Modeling experiment				
			M18E18	M19E19	M20E20	M21E20	M21E19
Goto	PM$_{2.5}$	R	0.83**	0.81**	0.76**	–	–
		NMB (%)	− 37.1	− 34.7	− 22.1*	–	–
		NME (%)	40.5*	40.3*	44.4*	–	–
	SO$_4^{2-}$	R	0.79**	0.76**	0.48*	–	–
		NMB (%)	− 25.6*	− 17.4*	− 3.2**	–	–
		NME (%)	38.4*	37.3*	59.3	–	–
	NO$_3^-$	R	0.57	0.60	0.83	–	–
		NMB (%)	− 51.2*	− 37.2*	− 32.8*	–	–
		NME (%)	70.6*	66.8*	63.7**	–	–
Tsushima	PM$_{2.5}$	R	–	–	0.71**	0.59*	**0.65***
		NMB (%)	–	–	− 22.6*	− 56.6	**− 46.5**
		NME (%)	–	–	48.5*	57.8	**49.6***
	SO$_4^{2-}$	R	–	–	0.55*	0.66*	**0.69***
		NMB (%)	–	–	− 2.1**	− 26.1*	**− 10.3***
		NME (%)	–	–	53.6	48.1*	**45.9***
	NO$_3^-$	R	–	–	0.81	0.65	**0.65**
		NMB (%)	–	–	− 22.9*	− 63.6*	**− 36.5***
		NME (%)	–	–	58.6**	73.0*	**63.8****
Oki	PM$_{2.5}$	R	0.75**	0.66*	0.48*	0.61*	**0.62***
		NMB (%)	− 29.3*	− 42.3	− 37.1	− 49.2	**− 36.8**
		NME (%)	39.1*	46.2*	54.0	54.5	**47.7***
	SO$_4^{2-}$	R	0.72**	0.71**	0.55*	0.71**	0.69*
		NMB (%)	− 20.0*	− 22.7*	− 10.8*	− 17.2*	**− 1.8****
		NME (%)	42.6*	35.8*	40.8*	38.1*	40.1*
	NO$_3^-$	R	0.51	0.54	0.56	0.50	**0.53**
		NMB (%)	− 16.9*	− 20.8*	− 32.5*	− 55.3*	**− 22.7***
		NME (%)	76.4*	70.1*	74.8*	75.2*	**74.8***

Table 2. Statistical analyses of modeling performance. Notes: for PM$_{2.5}$ and SO$_4^{2-}$, the model performance goals (marked by **) are $R > 0.70$, $NMB < \pm 10\%$ and $NME < +35\%$, and the model performance criteria (marked by *) are $R > 0.4$, $NMB < \pm 30\%$ and $NME < +50\%$; for NO$_3^-$, the model performance goals (marked by **) are $NMB < \pm 15\%$ and $NME < +65\%$, and the model performance criteria (marked by *) are $NMB < \pm 65\%$ and $NME < +115\%$[64]. Where M21E19 is superior to M21E20 in a statistical score, the value is given in bold font.

of supposing emission changes in 2021 can be estimated. From comparing the simulation results and the ACSA observations for Tsushima and Oki in 2021 (Fig. 2), the observations showed increases in PM$_{2.5}$ and NO$_3^-$ but almost none in SO$_4^{2-}$, whereas M21E20 showed decreases except for a slight increase in NO$_3^-$ at Oki. The results from M21E20 did not explain the variation observed in 2021, whereas M21E19 gave almost flat variations in PM$_{2.5}$ and SO$_4^{2-}$ and an increase in NO$_3^-$. The results from M21E19 were much closer to the observational results. The relative changes in the PM$_{2.5}$, SO$_4^{2-}$ and NO$_3^-$ concentrations after COVID-19 (Fig. 3) also clarified the differences in modeling performance for 2021. Experiment M21E20 showed negative changes after COVID-19 except for NO$_3^-$ at Oki, results that are not consistent with the observations, whereas M21E19 showed better agreement with the observations. These analyses show that M21E19 outperformed M21E20 in capturing the changes observed after COVID-19. In terms of statistical scores (Table 2), M21E19 also outperformed M21E20. These results clarify that the emission status in 2021 was not the same as during COVID-19 and was close to the status before COVID-19. Chinese economic activity and anthropogenic emissions recovered in 2021 and impacted the air quality in downwind regions through long-range PM$_{2.5}$ transport.

Note that experiment M21E20 gave negative changes after COVID-19. Based on the differences between M20E20 and M21E20 (i.e., the M21E20 results minus the M20E20 ones), the impact due to the meteorology and changes in natural emission in 2021 can be investigated. The impacts on air quality caused by the meteorological field have been reported with regard to chemical processes[27,28] and transport process[29]. The model-estimated changes in the concentrations of PM$_{2.5}$, SO$_4^{2-}$ and NO$_3^-$ caused by meteorology and natural emissions are shown in Fig. 4a–c. The negative changes in PM$_{2.5}$, SO$_4^{2-}$ and NO$_3^-$ concentrations over the East China Sea to the Korean Peninsula and western Japan are shown clearly (Fig. 4a–c). Based on the analyses of changes in natural emissions, volcanoes distributed mainly over the western island of Kyushu[30,31] showed SO$_2$ emissions of 605 Gg/period in 2020 and 307 Gg/period in 2021. This decrease could partly explain the negative change in 2021 as found in SO$_4^{2-}$, but a negative change in SO$_4^{2-}$ will lead to a positive change in NO$_3^-$ as examined previously as a paradigm shift in aerosol composition. Therefore, the negative changes seen for PM$_{2.5}$, SO$_4^{2-}$ and NO$_3^-$ can be attributed to changes in the meteorological field. To clarify this point, several meteorological fields are shown in Fig. S1 as
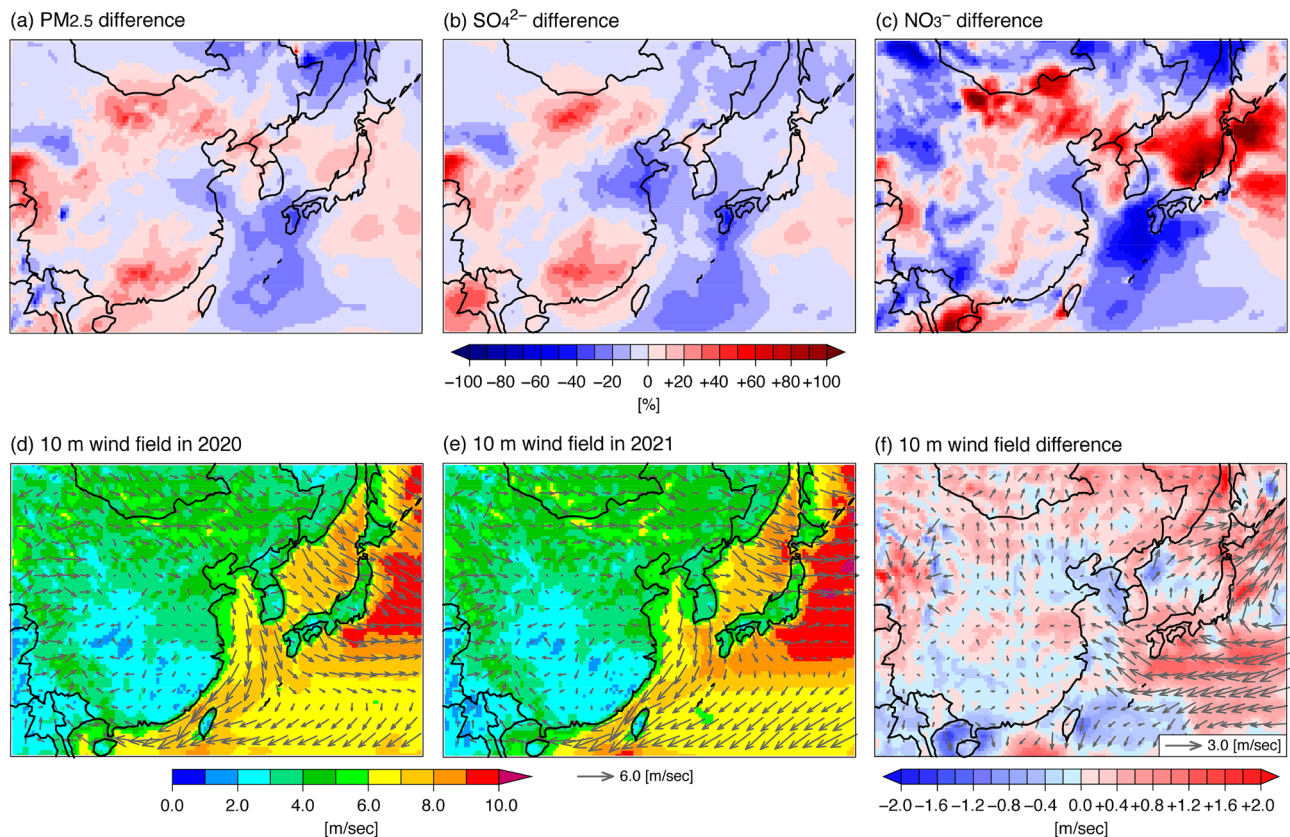
Figure 4. Changes in (**a**) PM$_{2.5}$, (**b**) SO$_4^{2-}$ and (**c**) NO$_3^-$ concentrations during and after COVID-19 due to meteorology and changes in natural emissions by calculating the M21E20 values minus the M20E20 ones. Modelled 10-m wind field (colour denotes 10-m wind speed) in (**d**) 2020 (M20) and (**e**) 2021 (M21), and change in 10-m wind field by calculating the M21 WRF meteorological field minus the M20 one. The analysed period is the average of February and March. The maps were generated with gtool3 (http://www.gfd-dennou.org/library/gtool/index.htm.en).

the difference between 2021 and 2020 (i.e., the M21 meteorological fields minus the M20 ones) overlaid with the observational results. The positive relative humidity over the East China Sea may enhance the aqueous-phase reaction of SO$_4^{2-}$ and did not relate to negative changes in PM$_{2.5}$ and SO$_4^{2-}$ (Fig. S1a). The change in precipitation was inhomogeneous over the East China Sea to western Japan (Fig. S1b). Lower planetary boundary layer (PBL) height found over oceans will lead to accumulated pollutants and did not explain the negative concentrations (Fig. S1c). The change in the 2-m temperature partly explains the NO$_3^-$ change as understood by thermodynamic NO$_3^-$ production. The positive and negative temperatures over western and eastern Japan (Fig. S1d) are generally consistent with the negative and positive changes in NO$_3^-$ concentration over these areas (Figs. 4c and S1d). The positive change in the 10-m wind speed could contribute to the negative changes in concentrations because of the faster transport of polluted air mass (Fig. S1e). The most plausible explanation comes from the change in the 10-m wind direction (Fig. S1f.), which was positive over eastern China to the East China Sea and western Japan. Further detailed illustrations of wind field are shown in Fig. 4d and e. During winter, the seasonal wind pattern is generally in the northwest direction[5], and a northwest wind direction was simulated over the East China Sea to western Japan in 2020 (Fig. 4d); however, a north wind direction dominated in 2021 over western Japan (Fig. 4e). Therefore, a positive difference in wind direction with positive wind speed was calculated over western Japan (Figs. 4f and S1e and f). The results observed at Tsushima and Oki are also displayed (Fig. S2), and the observations at Tsushima show clearly the change in wind direction from NNW in 2020 to N in 2021. The results of HYSPLIT backward trajectory[32] analyses from Goto are also presented (Fig. S3). These show the role of long-range transport from eastern China into western Japan during wintertime, and some trajectories were originated from northeastern China or eastern Japan in 2021; indicating the change of transport pattern in 2021 as also shown by simulated meteorological field (Figs. 4d and e and f). These findings suggest that the meteorological conditions in 2021—especially the wind direction—prevented long-range PM$_{2.5}$ transport. Nevertheless, the observations showed increases in PM$_{2.5}$ and NO$_3^-$ and almost no change in SO$_4^{2-}$ in 2021. This point supports the assertion that the changes in concentrations in 2021 cannot be explained without the returning impact of long-range PM$_{2.5}$ transport associated with the growth in Chinese anthropogenic emissions after COVID-19.

Finally, as an extension of the analysis in our previous study[4], the SO$_4^{2-}$ and NO$_3^-$ variations before, during and after COVID-19 are summarised in Fig. 5. The scatterplot of SO$_4^{2-}$/NO$_3^-$ at Goto from before to during COVID-19 has an inverted V shape. In this figure, the variations of SO$_4^{2-}$ and NO$_3^-$ reported as a paradigm shift in our previous study[4] are overlaid (grey open circles with a linear fitting line). These observation data[4]
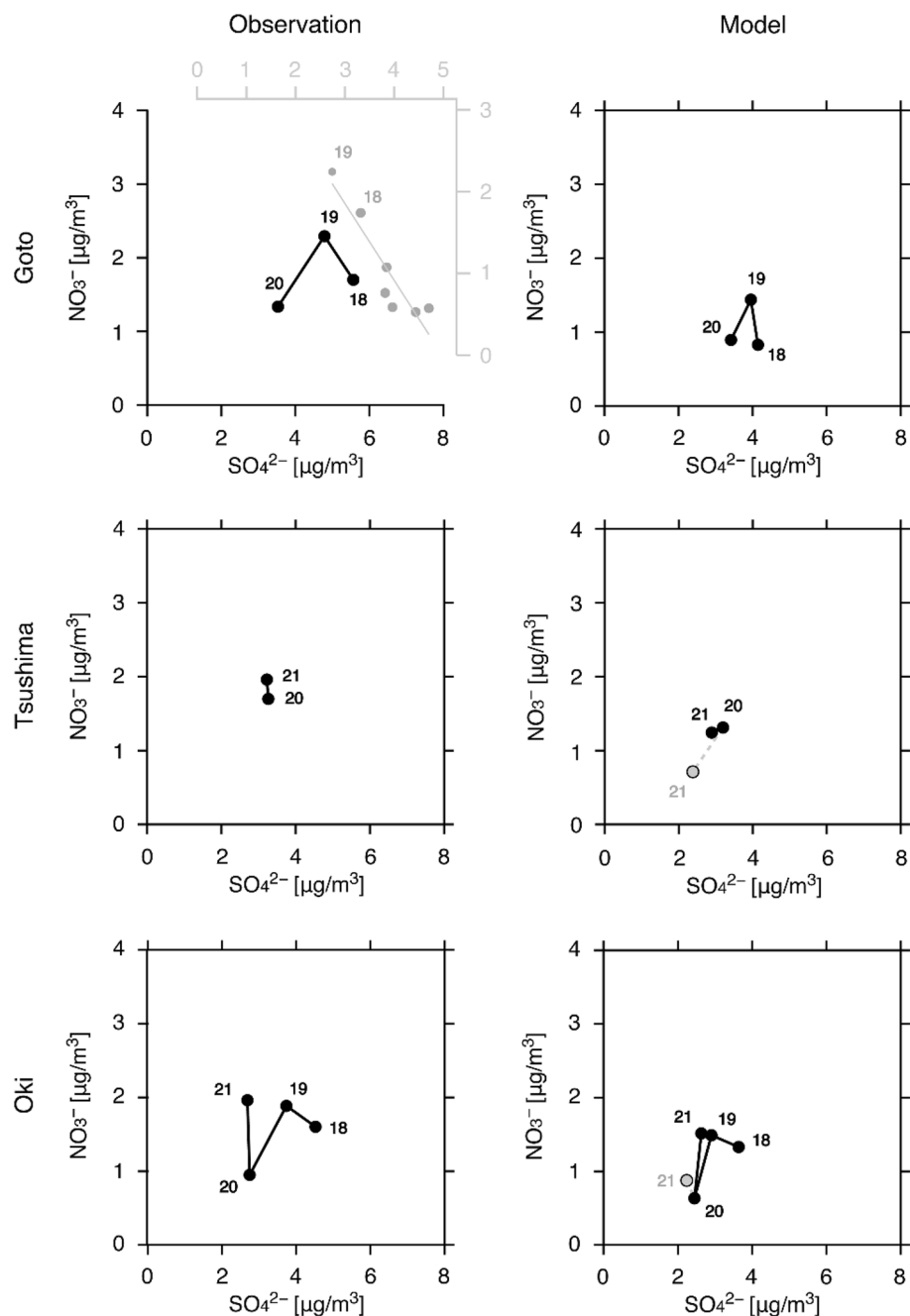
Figure 5. (Left) Observed and (right) modelled scatterplots of SO_4^{2-} and NO_3^- at (top) Goto, (middle) Tsushima and (bottom) Oki averaged over two months (February and March). The number near each circle indicates the year (i.e., '18' means 2018). At Goto, the results from a previous study[4] are shown in grey. The previous study analysed PM_1 components, whereas the present study analysed $PM_{2.5}$ components. For the model results, those of experiment M21E20 are shown by the grey closed circles.

were measured using a quadruple-type aerosol chemical speciation monitor (Q-ACSM) for fine aerosols of PM_1, whereas the present study analysed $PM_{2.5}$ components using an ACSA. The variations of SO_4^{2-} decrease and NO_3^- increase were also found based on ACSA observations up to 2019, and the dramatic decreases in both SO_4^{2-} and NO_3^- during COVID-19 were furthermore clarified in the present study. The modeling simulation also reproduced well this inverted V-shaped variation. At Tsushima, the variations from during COVID-19 to after COVID-19 were relatively small. From the observational results, SO_4^{2-} did not change but NO_3^- increased slightly, and the model results also show small variations. Note that experiment M21E20 (grey closed circles) gave deviations from these small variations in both SO_4^{2-} and NO_3^-. These results also show that assuming the emission status from during COVID-19 for 2021 was not appropriate. For further improvement of the modeling for Tsushima, the updated emission status over the Republic of Korea should be used. At Oki, the scatterplot

of SO_4^{2-}/NO_3^- from before to during COVID-19 also has an inverted V shape as found at Goto. The variation from during COVID-19 to after COVID-19 shows no change in SO_4^{2-} but an increase in NO_3^-. Experiment M21E19 reproduced this variation, but M21E20 did not. These analyses of the scatterplot of SO_4^{2-}/NO_3^- show substantial decreases in both SO_4^{2-} and NO_3^- during COVID-19 but suggest the return to the situation of aerosol composition change regarding the importance of NO_3^- after COVID-19 over the leeward of East Asia. The status of aerosol composition change should be monitored continuously because the nitrogen burden over East Asia is an issue of concern both currently and for the future[33,34]. The atmospheric input of nitrogen via dry and wet deposition processes over East Asia has been estimated in previous studies, and its significance has been clarified[35–38]. Targeting the proper management of nitrogen, the nitrogen burden during and after COVID-19 should be clarified in future work.

Methods

Observations. To obtain the spatial distribution of the NO_2 column, which can be regarded as a proxy for NO_x emissions[39], space-borne OMI measurements using the level-3 daily global nitrogen dioxide product (OMNO2d version 3.0) gridded into $0.25° \times 0.25°$[40] was used. We analysed the tropospheric column with clouds screened under the condition of a cloud fraction of less than 30%.

For ground-based observation of $PM_{2.5}$ and its components, ACSA observation datasets for 10 sites in Japan were available[41]. The Japanese Ministry of the Environment (MOE) created this observation network in April 2017, and two remote observation sites at Goto (128.65°E, 32.60°N) and Oki (133.20°E, 36.28°N), located in western Japan, were analysed in the present study. The ACSA measured $PM_{2.5}$ and the secondary inorganic components of SO_4^{2-} and NO_3^- with an hourly temporal resolution; this high temporal resolution minimises the effect of the volatilisation of NO_3^-[42]. Observations at the Goto site were unavailable from the autumn of 2020 onwards because of a typhoon; to compensate for these missing observations at Goto, observations at the Tsushima (129.29°E, 34.24°N) site were used for 2020 and 2021. The locations of the three sites at Goto, Tsushima and Oki are shown in Fig. 1c.

The lockdown in Wuhan began on 23 January 2020 and lasted until 8 April 2020, and those in other Chinese cities occurred within this period[43]. In Japan, a state of emergency was proclaimed for seven prefectures including Tokyo on 7 April 2020, and this was extended nationwide on 16 April 2020; it ended on 14 May 2020 for 39 prefectures except for mega-cities such as Osaka and Tokyo, and on 25 May 2020 for all prefectures in Japan[44]. Emission changes over Japan can be supposed to have been low from February to March. As also seen from the Stringency Index released from One World Data[45], the countermeasures against COVID-19 were the strictest in China from late January to the end of March, whereas other countries in East Asia had relatively loose measures in place during this period. Given these differences between China and Japan, the period analysed in the present study was chosen as February to March to focus on the variation of long-range $PM_{2.5}$ transport according to Chinese anthropogenic emissions.

Numerical modeling simulations. The numerical modeling simulations were performed using the regional chemical transport model of the Comprehensive Air quality Model with eXtensions (CAMx) version 6.4[46]. The simulation domain covering East Asia was configured by 215×120 grid points with 36-km horizontal resolution, centred at 116.2°E and 37.8°N on a Lambert conformal projection. The vertical resolution was 44 non-uniformly spaced layers from the surface to 50 hPa[37]. The meteorological fields to drive CAMx were calculated by the Weather Research and Forecasting (WRF) model version 4.1.1[47]. Gas-phase and aerosol chemistry were respectively adopted for SAPRC07TC[48,49] and the CF scheme in CAMx. Based on previous findings[50,51], the NO_2 aqueous-phase reaction in the SO_4^{2-} oxidation process was added. In addition, to enhance the production of SO_4^{2-} during winter haze events, the heterogeneous reaction of SO_2 on aerosol surfaces was introduced following the work on Chinese haze events[52]. The initial and lateral boundary conditions were prepared from winter-averaged values of the extended CMAQ model over the northern hemisphere[53].

In the present study, five modeling experiments were conducted, and the simulation setups are described in Table 1. In the names of these experiments, 'M' and 'E' stand for meteorology and anthropogenic emissions, respectively. For each year, the corresponding meteorological field generated by WRF was used. The emissions inventories were prepared as follows. Anthropogenic emissions except those in Japan and China were based on Hemispheric Transport of Air Pollution (HTAP) version 2.2[54]. For Japan, the latest available domestic emission inventory for 2015 developed by the MOE[55] was used. For China, the emission projections were based on the Multi-resolution Emission Inventory in China (MEIC). Trends in Chinese emissions up to 2017 have been reported[56], and their variation during the COVID-19 pandemic in 2020 have also been described[12]. Neither of those two references covered 2018, so instead the average data for 2017 and 2019 were calculated. From the MEIC estimations, the reduction in NO_x emissions in 2020 compared to those in 2019 during February and March was 36% and 14%, respectively, and the reduction in SO_2 emissions was 27% and 11%, respectively. NH_3 emissions were not provided for COVID-19[12], but because their main source is agriculture, we assumed that NH_3 emissions were unchanged during COVID-19[57] and we fixed them to the levels for 2017. Biogenic emissions were prepared from the Model of Emissions of Gases and Aerosols from Nature (MEGAN)[58] using the WRF-simulated meteorological field for the corresponding period. Biomass-burning emissions were taken from the beta version of the Global Fire Emissions Database (GFED) version 4.1[59]. SO_2 emissions from 15 volcanoes in Japan were prepared from a measurement report by the Japan Meteorological Agency (JMA)[60]. Sulphur emissions from ships could influence air quality, especially in areas close to the sea[61]. Because of the limited ship emission inventory, HTAP version 2.2 was used for 2018 and 2019, and a reduction in SO_2 emissions of 77% for 2020 and 2021 was applied based on a report by the International Maritime Organization (IMO)[62]. This reduction rate was consistent with a high-resolution emission inventory developed for Japan[63]. To our knowledge, the emission situation

in 2021—regarded as after the COVID-19 pandemic—is not yet available, so to consider the emission status in the region downwind of China from the observational facts, two experiments were conducted: (i) M21E20, which assumed the emission levels during COVID-19 for those in 2021, and (ii) M21E19, which assumed the emission levels before COVID-19 for those in 2021. By comparing these two experiments, the emission status in 2021 was investigated.

The model performance was evaluated statistically using the metrics of R, NMB and NME defined as

$$R = \frac{\sum_1^N (O_i - \overline{O})(M_i - \overline{M})}{\sqrt{\sum_1^N (O_i - \overline{O})^2}\sqrt{\sum_1^N (M_i - \overline{M})^2}}, \tag{3}$$

$$NMB = \frac{\sum_1^N (M_i - O_i)}{\sum_1^N O_i}, \tag{4}$$

$$NME = \frac{\sum_1^N |M_i - O_i|}{\sum_1^N O_i}, \tag{5}$$

where N is the total number of paired observations (O) and models (M), and these averages are denoted as $\overline{O}$ and $\overline{M}$, respectively. The recommended metrics based on a literature review for the United States[64] are given in Table 2.

Data availability
The datasets generated during and/or analysed during the current study are available from the corresponding author on reasonable request.

References
1. Dian, D., Xing, J., Wang, S. & Hao, J. Estimated contributions of emissions controls, meteorological factors, population growth, and changes in baseline mortality to reductions in ambient $PM_{2.5}$ and $PM_{2.5}$-related mortality in China, 2013–2017. *Environ. Health Perspect.* **127**, 067009. https://doi.org/10.1289/EHP4157 (2019).
2. Zhai, S. *et al.* Fine particulate matter ($PM_{2.5}$) trends in China, 2013–2018: Separating contributions from anthropogenic emissions and meteorology. *Atmos. Chem. Phys.* **19**, 11031–11041 (2019).
3. Zhang, Q. *et al.* Drivers of improved $PM_{2.5}$ air quality in China from 2013 to 2017. *Proc. Natl Acad. Sci. USA* **116**, 24463–24469. https://doi.org/10.1073/pnas.1907956116 (2019).
4. Uno, I. *et al.* Paradigm shift in aerosol chemical composition over regions downwind of China. *Sci. Rep.* **10**, 21748. https://doi.org/10.1038/s41598-020-63592-6 (2020).
5. Itahashi, S., Hayami, H., Yumimoto, K. & Uno, I. Chinese province-scale source apportionments for sulfate aerosol in 2005 evaluated by the tagged tracer method. *Environ. Poll.* **220**, 1366–1375. https://doi.org/10.1016/j.envpol.2016.10.098 (2017).
6. Itahashi, S. Toward synchronous evaluation of source apportionments for atmospheric concentration and deposition of sulfate aerosol over East Asia. *J. Geophys. Res. Atmos.* **123**, 2927–2953. https://doi.org/10.1002/2017JD028110 (2018).
7. Itahashi, S., Uno, I., Hayami, H. & Fujita, S. Modeling investigation of controlling factors in the increasing ratio of nitrate to non-seasalt sulfate in precipitation over Japan. *Atmos. Environ.* **92**, 171–177. https://doi.org/10.1016/j.atmosenv.2014.04.022 (2014).
8. Itahashi, S. *et al.* A 15-year record (2001–2015) of the ratio of nitrate to non-sea-salt sulfate in precipitation over East Asia. *Atmos. Chem. Phys.* **18**, 2835–2852. https://doi.org/10.5194/acp-18-2835-2018 (2018).
9. Huang, C. *et al.* Clinical features of patients infected with 2019 novel coronavirus in Wuhan, China. *Lancet* **395**, 497–506. https://doi.org/10.1016/S0140-6736(20)30183-5 (2020).
10. Chinazzi, M. *et al.* The effect of travel restrictions on the spread of the 2019 novel coronavirus (COVID-19) outbreak. *Science* **368**, 395–400. https://doi.org/10.1126/science.aba9757 (2020).
11. Tian, H. *et al.* An investigation of transmission control measures during the first 50 days of the COVID-19 epidemic in China. *Science* **368**, 638–642. https://doi.org/10.1126/science.abb6105 (2020).
12. Zheng, B. *et al.* Changes in China's anthropogenic emissions and air quality during the COVID-19 pandemic in 2020. *Earth Syst. Sci. Data* **13**, 2895–2907. https://doi.org/10.5194/essd-13-2895-2021 (2021).
13. Liu, F. *et al.* Abrupt decline in tropospheric nitrogen dioxide over China after the outbreak of COVID-19. *Sci. Adv.* **6**, eabc2992. https://doi.org/10.1126/sciadv.abc2992 (2020).
14. Huang, G. & Sun, K. Non-negligible impacts of clean air regulations on the reduction of tropospheric NO_2 over East China during the COVID-19 pandemic observed by OMI and TROPOMI. *Sci. Tot. Environ.* **745**, 141023. https://doi.org/10.1016/j.scitotenv.2020.141023 (2020).
15. Griffith, S. M. *et al.* Long-range air pollution transport in East Asia during the first week of the COVID-19 lockdown in China. *Sci. Tot. Env.* **741**, 140214. https://doi.org/10.1016/j.scitotenv.2020.140214 (2020).
16. Wang, Z. *et al.* Impacts of COVID-19 lockdown, Spring Festival and meteorology on the NO_2 variations in early 2020 over China based on in-situ observations, satellite retrievals and model simulations. *Atmos. Environ.* **244**, 117972. https://doi.org/10.1016/j.atmosenv.2020.117972 (2021).
17. Wu, S. *et al.* Spatiotemporal mapping and assessment of daily ground NO_2 concentrations in China using high-resolution TROPOMI retrievals. *Environ. Poll.* **273**, 116456. https://doi.org/10.1016/j.envpol.2021.116456 (2021).
18. Wang, Y. *et al.* Changes in air quality related to the control of coronavirus in China: Implications for traffic and industrial emissions. *Sci. Total Environ.* **731**, 139133. https://doi.org/10.1016/j.scitotenv.2020.139133 (2020).
19. Bao, R. & Zhang, A. Does lockdown reduce air pollution? Evidence from 44 cities in northern China. *Sci. Total Environ.* **731**, 139052. https://doi.org/10.1016/j.scitotenv.2020.139052 (2020).
20. Chatani, S., Shimadera, H., Itahashi, S. & Yamaji, K. Comprehensive analyses of source sensitivities and apportionments of $PM_{2.5}$ and ozone over Japan via multiple numerical techniques. *Atmos. Chem. Phys.* **20**, 10311–10329. https://doi.org/10.5194/acp-20-10311-2020 (2020).

21. Liu, J., Li, J. & Yao, F. Source-receptor relationship of transboundary particulate matter pollution between China, South Korea and Japan: Approaches, current understanding and limitations. *Crit. Rev. Environ. Sci. Technol.* https://doi.org/10.1080/10643389.2021.1964308ERL (2021).

22. International Monetary Fund. World economic outlook: Recovery during a pandemic—Health concerns, supply disruptions, price pressures. Report at https://www.imf.org/-/media/Files/Publications/WEO/2021/October/English/text.ashx (2021).

23. Chatani, S., Itahashi, S. & Yamaji, K. Advantages of continuous monitoring of hourly PM$_{2.5}$ component concentrations in Japan for model validation and source sensitivity analyses. *Asian. J. Atmos. Environ.* **215**, 2021008. https://doi.org/10.5572/ajae.2021.008 (2021).

24. Liu, T., Chan, A. W. H. & Abbatt, J. P. D. Multiphase oxidation of sulfur dioxide in aerosol particles: Implications for sulfate formation in polluted environments. *Env. Sci. Tech.* **55**, 4227–4242. https://doi.org/10.1021/acs.est.0c06496 (2021).

25. Itahashi, S. *et al.* Model performance differences in fine-mode nitrate aerosol during wintertime over Japan in the J-STREAM model inter-comparison study. *Atmosphere* **11**, 511. https://doi.org/10.3390/atmos11050511 (2020).

26. Uno, I. *et al.* Seasonal variation of fine- and coarse-mode nitrates and related aerosols over East Asia: Synergetic observations and chemical transport model analysis. *Atmos. Chem. Phys.* **17**, 14181–14197. https://doi.org/10.5194/acp-17-14181-2017 (2017).

27. Le, T. *et al.* Unexpected air pollution with marked emission reductions during the COVID-19 outbreak in China. *Science* **369**, 702–706. https://doi.org/10.1126/science.abb7431 (2020).

28. Liu, L. *et al.* Chemistry of atmospheric fine particles during the COVID-19 pandemic in a megacity of eastern China. *Geophys. Res. Lett.* **48**, e2020GL091611. https://doi.org/10.1029/2020GL091611 (2021).

29. Zhang, J. *et al.* Trans-regional transport of haze particles from the North China Plain to Yangtze River Delta during winter. *J. Geophys. Res. Atmos.* **126**, e2020JD033778. https://doi.org/10.1029/2020JD033778 (2021).

30. Itahashi, S. *et al.* Model estimation of sulfate aerosol sources collected at Cape Hedo during an intensive campaign in October-November, 2015. *Aerosol Air Qual. Res.* **17**, 3079–3090. https://doi.org/10.4209/aaqr.2016.12.0592 (2017).

31. Yamamura, Y. *et al.* Contribution of volcanic SO$_2$ emission to high concentration PM$_{2.5}$ under summertime Pacific High condition. *J. Jpn. Soc. Atmos. Environ.* **55**, 169–180 (2020) (in Japanese with English abstract).

32. National Oceanic and Atmospheric Administration. HYSPLIT. https://www.ready.noaa.gov/HYSPLIT.php (n.d.).

33. Bleeker, A., Hicks, W. K., Dentener, F., Galloway, J. & Erisman, J. W. N deposition as a threat to the World's protected area under the Convention of Biological Diversity. *Env. Poll.* **159**, 2280–2288. https://doi.org/10.1016/j.envpol.2010.10.036 (2011).

34. Sutton, M. A. & Bleeker, A. The shape of nitrogen to come. *Nature* **494**, 435–437 (2013).

35. Itahashi, S., Hayami, H., Uno, I., Pan, X. & Uematsu, M. Importance of coarse-mode nitrate produced via sea salt as atmospheric input to East Asian oceans. *Geophys. Res. Lett.* **43**, 5483–5491. https://doi.org/10.1002/2016GL068722 (2016).

36. Itahashi, S. *et al.* MICS-Asia III: overview of model intercomparison and evaluation of acid deposition over Asia. *Atmos. Chem. Phys.* **20**, 2667–2693. https://doi.org/10.5194/acp-20-2667-2020 (2020).

37. Itahashi, S. *et al.* Nitrogen burden from atmospheric deposition in East Asian oceans in 2010 based on high-resolution regional numerical modeling. *Env. Poll.* **486**, 117309. https://doi.org/10.1016/j.envpol.2021.117309 (2021).

38. Ge, B. *et al.* Model Inter-Comparison Study for Asia (MICS-Asia) phase III: Multimodel comparison of reactive nitrogen deposition over China. *Atmos. Chem. Phys.* **20**, 10587–10610. https://doi.org/10.5194/acp-20-10587-2020 (2020).

39. Itahashi, S. *et al.* Inverse estimation of NO$_x$ emissions over China and India 2005–2016: contrasting recent trends and future perspectives. *Environ. Res. Lett.* **14**, 124020. https://doi.org/10.1088/1748-9326/ab4d7f (2019).

40. Nickolay A. *et al.* OMI/Aura NO$_2$ Cloud-Screened Total and Tropospheric Column L3 Global Gridded 0.25 degree × 0.25 degree V3. *NASA Goddard Space Flight Center, Goddard Earth Sciences Data and Information Services Center (GES DISC)* https://doi.org/10.5067/Aura/OMI/DATA3007 (2019).

41. Ministry of the Environment. http://www.env.go.jp/air/%20osen/pm_resultmonitoring/post_25.html (n.d.) (in Japanese).

42. Itahashi, S. *et al.* Nitrate transboundary heavy pollution over East Asia in winter. *Atmos. Chem. Phys.* **17**, 3823–3843. https://doi.org/10.5194/acp-17-3823-2017 (2017).

43. Lai, S. *et al.* Effect of non-pharmaceutical interventions to contain COVID-19 in China. *Nature* **585**, 410–413. https://doi.org/10.1038/s41586-020-2293-x (2020).

44. Cabinet Secretariat of Japan. COVID-19 information and resources. https://corona.go.jp/en/ (n.d.)

45. One World Data. COVID-19: Stringency index. https://ourworldindata.org/covid-stringency-index (2020).

46. Ramboll Environment and Health. *User's guide, comprehensive air quality model with extensions version 6.40* (Ramboll, 2016).

47. Skamarock, W. C. *et al.* *A description of the advanced research WRF version 4. NCAR Tech. Note, NCAR/TN-556+STR.* 162 (National Center for Atmospheric Research, Boulder, 2019)

48. Carter, W. P. L. Development of the SAPRC-07 chemical mechanism. *Atmos. Environ.* **44**, 5324–5335 (2010).

49. Hutzell, W. T., Luecken, D. J., Appel, W. K. & Carter, W. P. Interpreting predictions from the SAPRC07 mechanism based on regional and continental simulations. *Atmos. Environ.* **46**, 417–429 (2012).

50. Itahashi, S. *et al.* Model performance differences in sulfate aerosol in winter over Japan based on regional chemical transport models of CMAQ and CAMx. *Atmosphere* **9**, 488. https://doi.org/10.3390/atmos9120488 (2018).

51. Itahashi, S., Uchida, R., Yamaji, K. & Chatani, S. Year-round modeling of sulfate aerosol over Asia through updates of aqueous-phase oxidation and gas-phase reactions with stabilized Criegee intermediates. *Atmos. Environ. X.* **12**, 100123. https://doi.org/10.1016/j.aeaoa.2021.100123 (2021).

52. Zheng, B. *et al.* Heterogeneous chemistry: a mechanism missing in current models to explain secondary inorganic aerosol formation during the January 2013 haze episode in North China. *Atmos. Chem. Phys.* **15**, 2031–2049. https://doi.org/10.5194/acp-15-2031-2015 (2015).

53. US EPA. Hemispheric CMAQ model version 5.3beta output data—2016 seasonally averaged 108km for N. hemisphere, UNC Dataverse, V1. Dataset at https://doi.org/10.15139/S3/QJDYWO (2019)

54. Janssens-Maenhout, G. *et al.* HTAP_v2.2: A mosaic of regional and global emission grid maps for 2008 and 2010 to study hemispheric transport of air pollution. *Atmos. Chem. Phys.* **15**, 11411–11432. https://doi.org/10.5194/acp-15-11411-2015 (2015).

55. Zheng, B. *et al.* Trends in China's anthropogenic emissions since 2010 as the consequence of clean air actions. *Atmos. Chem. Phys.* **18**, 14095–14111. https://doi.org/10.5194/acp-18-14095-2018 (2018).

56. Ministry of Environment. PM$_{2.5}$ emission inveotory. http://www.env.go.jp/air/osen/pm/info.html#INVENTORY (n.d.) (in Japanese).

57. Forster, P. M. *et al.* Current and future global climate impacts resulting from COVID-19. *Nat. Clim. Change* **10**, 913–919. https://doi.org/10.1038/s41558-020-0883-0 (2020).

58. Guenther, A. B. *et al.* The Model of Emissions of Gases and Aerosols from Nature version 2.1 (MEGAN2.1). An extended and updated framework for modeling biogenic emissions. *Geosci. Model Dev.* **5**, 1471–1492. https://doi.org/10.5194/gmd-5-1471-2012 (2012).

59. van der Werf, G. R. *et al.* Global fire emissions estimates during 1997–2016. *Earth Syst. Sci. Data* **9**, 697–720. https://doi.org/10.5194/essd-9-697-2017 (2017).

60. Japan Meteorological Agency. Activity of each volcano. http://www.data.jma.go.jp/svd/vois/data/tokyo/volcano.html (n.d.) (in Japanese).

61. Itahashi, S., Sakurai, T., Shimadera, H., Araki, S. & Hayami, H. Long-term trends of satellite-based fine-mode aerosol optical depth over the Seto Inland Sea, Japan, over two decades (2001–2020). *Environ. Res. Lett.* **16**, 064062. https://doi.org/10.1088/1748-9326/ac03db (2021).
62. International Maritime Organization. Air pollution and energy efficiency: Study on the effects of the entry into force of the global 0.5% fuel oil sulphur content limit on human health. https://edocs.imo.org/Final Documents/English/MEPC 70-INF.34 (E).docx (2016).
63. Sakurai, T., Ito, M. & Hanayama, S. Development of air pollutants emission inventories for ships around Japan on a high geographical resolution. *Asian J. Atmos. Environ.* **15**, 2020096. https://doi.org/10.5572/ajae.2020.096 (2021).
64. Emery, C. *et al.* Recommendations on statistics and benchmarks to assess photochemical model performance. *J. Air Waste Manag. Assoc.* **67**, 582–598. https://doi.org/10.1080/10962247.2016.1265027 (2017)

Acknowledgements

Author contributions

S.I. conducted the model simulations and analysed the model results, surface observations and satellite measurements. Y.Y. conducted the surface observations at the Tsushima site and analysed the observation dataset. Z.W. and I.U. conducted the analyses of the surface observations. S.I. and I.U. designed the study and also wrote the manuscript with valuable input from all co-authors. All authors reviewed the manuscript.

Competing interests

The authors declare no competing interests.

Additional information

Supplementary Information The online version contains supplementary material available at https://doi.org/10.1038/s41598-022-09388-2.

Correspondence and requests for materials should be addressed to S.I.

Reprints and permissions information is available at www.nature.com/reprints.

Publisher's note Springer Nature remains neutral with regard to jurisdictional claims in published maps and institutional affiliations.